Aerosols chemical composition, light extinction, and source apportionment near a desert margin city, Yulin, China

Yali Lei[1], Zhenxing Shen[1], Zhuoyue Tang[1], Qian Zhang[2], Jian Sun[1], Yongjing Ma[3,4], Xiaoyan Wu[3,4], Yiming Qin[5], Hongmei Xu[1] and Renjian Zhang[6]

[1] Department of Environmental Sciences and Engineering, Xi'an Jiaotong University, Xi'an, Shaanxi, China
[2] School of Environmental & Municipal Engineering, Xi'an University of Architecture and Technology, Xi'an, Shaanxi, China
[3] College of Atmospheric Sciences, Key Laboratory of Arid Climatic Change and Reducing Disaster of Gansu Province, Lanzhou University, Lanzhou, China
[4] State Key Laboratory of Atmospheric Boundary Layer Physics and Atmospheric Chemistry (LAPC), Institute of Atmospheric Physics, Chinese Academy of Sciences, Beijing, China
[5] School of Engineering and Applied Sciences, Harvard University, Cambridge, United States of America
[6] Key Laboratory of Regional Climate-Environment Research for Temperate East Asia, Institute of Atmospheric Physics, Chinese Academy of Sciences, Beijing, China

Corresponding authors
Zhenxing Shen,
zhenxingshen@163.com,
zxshen@mail.xjtu.edu.cn
Renjian Zhang, zrj@mail.iap.ac.cn

ABSTRACT

Daily PM_{10} and $PM_{2.5}$ sampling was conducted during four seasons from December 2013 to October 2014 at three monitoring sites over Yulin, a desert margin city. PM_{10} and $PM_{2.5}$ levels, water soluble ions, organic carbon (OC), and elemental carbon (EC) were also analyzed to characterize their chemical profiles. b_{ext} (light extinction coefficient) was calculated, which showed the highest in winter with an average of $232.95 \pm 154.88 \ Mm^{-1}$, followed by autumn, summer, spring. Light extinction source apportionment results investigated $(NH_4)_2SO_4$ and NH_4NO_3 played key roles in the light extinction under high RH conditions during summer and winter. Sulfate, nitrate and Ca^{2+} dominated in $PM_{10}/PM_{2.5}$ ions. Ion balance results illustrated that PM samples were alkaline, and PM_{10} samples were more alkaline than $PM_{2.5}$. High SO_4^{2-}/K^+ and Cl^-/K^+ ratio indicated the important contribution of coal combustion, which was consistent with the OC/EC regression equation intercepts results. Principal component analysis (PCA) analyses results showed that the fugitive dust was the most major source of PM, followed by coal combustion & gasoline vehicle emissions, secondary formation and diesel vehicle emissions. Potential contribution source function (PSCF) results suggested that local emissions, as well as certain regional transport from northwesterly and southerly areas contributed to $PM_{2.5}$ loadings during the whole year. Local government should take some measures to reduce the PM levels.

INTRODUCTION

Atmospheric aerosols have been found to be associated with adverse influences on atmospheric visibility, human health, and global climate change (*Watson, 2002*; *Yuan et al.,*

2006; *Cao et al., 2009*; *Huang et al., 2014*). Aerosol extinction (scattering and absorption) plays the key role in the earth system (such as, radiative balance and energy budget) (*Charlson et al., 1992*). Chemical components of PM contributed to extinction can establish control measurement to alleviate visibility degradation (*Tao et al., 2015*). Sulfate, nitrate, organic matter (OM) and elemental carbon (EC) have been considered as dominant components of PM (*Cao et al., 2003*; *Shen et al., 2014*). All of the chemical compounds contributed to visibility degradation (*Lee et al., 2009*).

   Yulin ($36.95°-39.58°N$, $107.46°-111.25°E$), located in the Mu Us Desert, is one of the Asian Pacific Regional Aerosol Characterization Experiment (ACE-Asia) super site. However, most studies carried in Yulin have been studied to determine the chemical and physical profiles of Asian dust and its transportation (*Xu et al., 2004*). As the national energy and chemical industrial base, fossil fuel consumption and motor vehicles have rapidly increased in Yulin because of the economic growth, population expansion and urbanization. Actually, a study has been conducted recently aiming to understand brown carbon (BrC) can be also emitted from coal combustion in Yulin (*Lei et al., 2018*). However, seasonal PM levels, chemical species and visibility degradation are still lacking. It is not known dominant chemical components to light extinction during different seasons. Such information will offer practical and significant values in making relevant control to increase the atmospheric visibility. In this study, PM sampling was conducted in three represented sites for one year, and water-soluble ions and carbonaceous species (OC/EC) were also measured to understand PM pollution and their potential sources.

MATERIALS & METHODS

Sample collection

Samplings were conducted at three sites (Fig. 1): Environmental Monitoring Station (EMS) is a mixed commercial-residential-traffic site; Experimental High School (EHS) represents a residential site, and Environmental Protection Agency (EPA) is considered as rural areas. All the sampling sites have been permitted and coordinated by the Yulin Environmental Monitoring Station. We selected four months for each season which were winter (December 2013), spring (April 2014), summer (July 2014), October (autumn 2014). PM samples were collected by six mini-volume samplers (Airmetrics, Springfield, OR) at 5 L min^{-1}. Table S1 listed the sampling information about characteristics of the PM fraction sampling measurements. 121 PM$_{10}$ and 285 PM$_{2.5}$ samples were collected onto 47-mm quartz microfiber filters (Whatman, Maidstone, UK) using six minivolume samplers (Airmetrics, Springfield, OR) at 5 L/min. Before sampling, the quartz filters were pre-heated to 800 °C for 3 h to remove any residual carbon. After sampling, the filters were placed in clean plastic cassettes and stored in a refrigerator at $\sim$4 °C until in order to minimize the evaporation of volatile components. More details can be found in *Lei et al. (2018)*.

Mass and chemical analysis

PM samples were equilibrated using controlled temperature (20–23 °C) and relative humidity (35–45%) desiccators for 24 h before and after sampling, and their mass loadings were determined gravimetrically using a Sartorius MC5 electronic microbalance ($\pm$1 μg
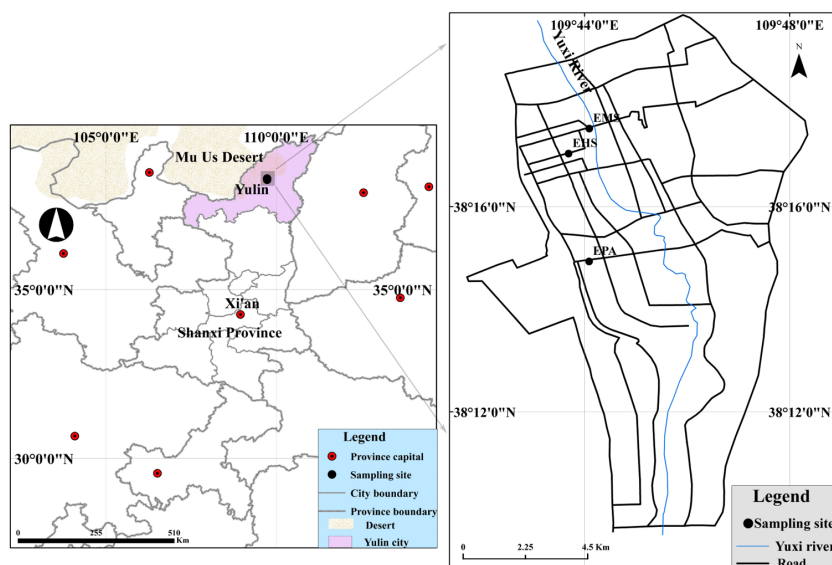
Figure 1 **Locations of the monitoring sites and surrounding region.**

sensitivity; Sartorius, Göttingen, Germany). Each filter was weighed at least three times before and after sampling after 24 h equilibration period. The differences among the three repeated weightings typically were less than 10 μg for blanks and 15 μg for sample filters. 1/4 of each filter sample was extracted by 10 mL distilled-deionized water (18.2 M Ω) to analyze ions. Cations were detected by a CS12A column (Dionex Co., Sunnyvale, CA) and 20 mM methanesulfonate as an eluent. Anions were separated by an AS11-HC column (Dionex Co., Sunnyvale, CA) using 20 mM KOH as the eluent with detection limits less than 0.05 mg/L (*Chow & Watson, 1999*). Standard reference materials produced by the National Research Center for Certified Reference Materials, China, were analyzed for quality assurance purposes. Blank values were subtracted from sample concentrations. One sample in each group of ten samples was selected to analyze twice for quality control purposes. Additional details of ions analysis can be found in *Shen et al. (2008)*. OC and EC were analyzed using DRI Model 2001 Thermal/Optical Carbon Analyzer (Atmoslytic Inc., Calabasas, CA, USA) based on the thermal/optical reflectance (TOR) method (*Chow et al., 2007*). The analyzer was calibrated with CH_4 daily. One replicate analysis was performed for each of 10 samples.

Data analysis
Neutralization factor
The neutralization factor (NF) can be used to describe the interaction between cations and anions (*Shen et al., 2012*). The NF of NH_4^+, Ca^{2+}, Mg^{2+} have been calculated using the formula below

$$NF_x = \frac{X}{NO_3^- + SO_4^{2-}} \qquad (1)$$

Where X may be NH_4^+, Ca^{2+} or Mg^{2+}, using their equivalent concentrations (microgram per cubic meter).

Light extinction source apportionment

The light extinction coefficient (b_{ext}), is calculated as the $PM_{2.5}$ scattering (b_{sp}, *Chow et al., 2002*), $PM_{2.5}$ absorption (b_{ap}, *Chow et al., 2010*), gas (NO_2) absorption (b_{ag}, *Hodkinson, 1966*), and Rayleigh scattering (b_{sg}, *Cao et al., 2012b*), where:

$$b_{ext} = b_{sp} + b_{ap} + b_{ag} + b_{sg} \tag{2}$$

$$b_{ap} = 10 \times [EC] \tag{3}$$

$$b_{ag} = 0.33 \times [NO_2] \tag{4}$$

$$b_{sp,wet} = f(RH) \times b_{sp,dry} \tag{5}$$

b_{ext} values can be approximately using the visual range (VR) (*Koschmieder, 1924*)

$$VR = \frac{3.912}{b_{ext}} \tag{6}$$

The revised IMPROVE formula was described as follow (*Pitchford et al., 2007*):

$$
\begin{aligned}
b_{ext} =\ & 2.2 \times f_s(RH)[(NH_4)_2SO_{4small}] + 4.8 \times f_s(RH)[(NH_4)_2SO_{4large}] \\
& + 2.4 \times f_s(RH)[NH_4NO_{3small}] + 5.1 \times f_L(RH) \times [NH_4NO_{3large}] + 2.8 \times [OM_{small}] \\
& + 6.1 \times [OM_{large}] + 10 \times [EC] + 1 \times [\text{soil dust}] + 1.7 \times f_{ss}(RH) \times [\text{seasalt}] \\
& + 0.6 \times [\text{coarse mass}] + 0.33 \times [NO_2] + \text{Rayleigh scattering(site specific)}
\end{aligned}
\tag{7}
$$

The Large sulfate ($sulfate_{large}$) and Small sulfate ($sulfate_{small}$) are accumulated using the IMPROVE equation (*John et al., 1990*):

$$[(NH_4)_2SO_{4large}] = \frac{[(NH_4)_2SO_{4Total}]^2}{20} \qquad \text{for } [(NH_4)_2SO_{4Total}] < 20\ \mu g m^{-3} \tag{8}$$

$$[(NH_4)_2SO_{4large}] = [(NH_4)_2SO_{4Total}] \qquad \text{for } [(NH_4)_2SO_{4Total}] \geq 20\ \mu g m^{-3} \tag{9}$$

$$[(NH_4)_2SO_{4small}] = [(NH_4)_2SO_{4Total}] - [(NH_4)_2SO_{4large}] \tag{10}$$

The soil fraction was estimated as follows (*Taylor & McLenna, 1985*):

$$[\text{soil dust}] = (\frac{1}{0.035}) \times [Fe] = 28.57 \times [Fe] \tag{11}$$

Potential contribution source function method

Potential contribution source function (PSCF) is in view of backward trajectories which connects the residence time in upwind areas with relative high concentrations of a certain species through conditional probabilities (*Polissar, Hopke & Harris, 2001*). The PSCF method can be described as follows:

$$PSCF(i,j) = w_{ij} \times (\frac{m_{ij}}{n_{ij}}) \tag{12}$$

where w_{ij} is an arbitrary weight function to decrease small values effect of n_{ij}. n_{ij} the number of the end points; m_{ij} is the number of trajectory end points in this grid cell whose values higher than the threshold value. In addition, the airmass backward trajectories had been previously calculated based on the National Oceanic and Atmospheric Administration (NOAA) Hybrid Single-Particle Lagrangian Integrated Trajectory model (*Ji et al., 2019*).

Principal component analysis (PCA) model

PCA is used to investigate the correlations among concentrations of chemical species at the receptor. The principal chemical species suggested the chemical species data variance and relevant possible sources (*Viana et al., 2006*; *Meng et al., 2015*). Each factor showed the maximum total variance of the data set and this set is completely uncorrelated with the rest of the data. The factor loadings obtained after the varimax rotation gives the correlation between the variables and the factor (*Cao et al., 2005*). SPSS^{TM} and Statgraphics can be utilized to perform multivariate factor analysis. As elements are treated equally no matter their concentrations, original variables should be normalized as follows:

$$Z_{ij} = \frac{(x_{ij} - \overline{x}_i)}{\sigma_i} \tag{13}$$

Where x_{ij} is the i th mass concentration of each specie measured in the j th sample; x_i is the average i th element mass concentration and σ_i is the standard deviation.

For each source PCA identified, the weighted regression of each PM fraction's concentration on the predicted PM contribution yields estimates of the content of that fraction in each source. More detailed introduction of this analysis method can be found in *Cao et al. (2005)*.

Meteorological data

Meteorological data, including ambient temperature, relative humidity (RH), wind speed (WS), and atmospheric pressure, were collected from Weather Underground (http://www.wunderground.com/).

RESULTS

Chemical composition in PM

Annual PM and chemical species in Yulin are summarized in Table 1. Generally, the yearly mean levels of PM_{10} and $PM_{2.5}$ were 121.5 μg m^{-3} and 65.0 μg m^{-3}. PM_{10} OC and EC levels were 17.9 μg m^{-3} and 5.5 μg m^{-3}; for $PM_{2.5}$, the values were 13.8 μg m^{-3} and 4.0 μg m^{-3}. The total ions levels of PM_{10} and $PM_{2.5}$ were 34.6 μg m^{-3} and 25.9 μg m^{-3}, which accounted for 28.4% and 39.9% of the PM_{10} and $PM_{2.5}$ mass, indicating that water-soluble ions comprise a large part of aerosol particles. The spatial distribution pattern showed that the PM_{10} and $PM_{2.5}$ levels at EPA were the lowest compared with EMS and EHS. OC and EC levels showed a similar spatial distribution pattern as the PM levels, that's EMS >EHS >EPA. In addition, the total ions levels at EMS (35.4 μg m^{-3} for PM_{10} and 26.1 μg m^{-3} for $PM_{2.5}$) and EHS (35.7 μg m^{-3} for PM_{10} and 26.8 μg m^{-3} for $PM_{2.5}$) were higher than those at EPA (32.1 μg m^{-3} for PM_{10} and 24.9 μg m^{-3} for $PM_{2.5}$). Sulfate, the most abundance component in PM, followed by Ca^{2+} and NO_3^{-}.

Table 1 Mass concentrations of PM and chemical species (Unit: $\mu g\,m^{-3}$).

PM Fraction			Mass	Na$^+$	NH$_4^+$	K$^+$	Mg^{2+}	Ca^{2+}	F$^-$	Cl$^-$	NO$_3^-$	SO$_4^{2-}$	OC	EC	OC/EC
EMS	PM$_{10}$	mean	135.9	3.7	2.4	0.7	0.5	7.4	0.3	3.0	5.5	12.1	21.3	6.6	3.4
	($n = 40$)	SD	70.2	1.2	2.0	0.4	0.4	3.9	0.2	3.1	3.2	5.5	12.5	3.7	1.2
	PM$_{2.5}$	mean	74.8	3.3	2.4	0.6	0.3	3.4	0.3	2.3	4.0	9.5	14.9	4.4	3.7
	($n = 95$)	SD	32.9	0.9	2.3	0.3	0.2	1.9	0.2	1.7	3.3	5.5	6.6	2.3	1.0
EHS	PM$_{10}$	mean	120.2	3.8	2.8	0.8	0.5	5.8	0.3	2.8	6.2	12.7	17.9	5.4	3.6
	($n = 41$)	SD	68.9	1.9	2.9	0.7	0.4	3.4	0.2	3.5	5.2	7.8	10.5	3.3	1.3
	PM$_{2.5}$	mean	63.0	3.4	2.8	0.6	0.2	2.5	0.3	2.4	4.3	10.2	14.5	4.0	4.1
	($n = 98$)	SD	26.2	1.0	2.4	0.3	0.2	1.3	0.2	2.3	3.5	5.8	7.8	2.6	1.4
EPA	PM$_{10}$	mean	108.4	3.5	2.3	0.6	0.5	5.7	0.3	2.1	5.6	11.7	14.6	4.6	3.5
	($n = 40$)	SD	64.4	1.2	1.9	0.3	0.3	3.2	0.3	2.2	3.3	6.1	6.9	2.4	1.6
	PM$_{2.5}$	mean	57.0	3.3	2.5	0.6	0.2	2.6	0.3	1.8	4.1	9.6	11.9	3.5	3.8
	($n = 92$)	SD	25.2	0.9	2.3	0.3	0.2	1.3	0.2	1.6	3.5	5.6	5.3	2.0	1.3
Average	PM$_{10}$	mean	121.5	3.6	2.5	0.7	0.5	6.3	0.3	2.6	5.8	12.2	17.9	5.5	3.5
	($n = 121$)	SD	68.3	1.5	2.3	0.5	0.4	3.5	0.2	3.0	4.0	6.5	10.5	3.3	1.4
	PM$_{2.5}$	mean	65.0	3.3	2.6	0.6	0.2	2.8	0.3	2.2	4.1	9.8	13.8	4.0	3.9
	($n = 285$)	SD	29.2	1.0	2.3	0.3	0.2	1.6	0.2	1.9	3.4	5.6	6.8	2.4	1.3

Seasonal variations of PM, OC, EC, three major ions Ca^{2+}, NO$_3^-$, and SO$_4^{2-}$ were shown in Fig. 2. In general, all the species were highest during winter but lowest during summer. During spring, PM$_{10}$ and PM$_{2.5}$ mean levels for dust dominated days were 283.4 $\mu g\,m^{-3}$ and 130.4 $\mu g\,m^{-3}$, which were both over 1.7 times of the spring average values. Two dust events were observed in winter and spring, leading the yearly highest PM$_{10}$ Ca^{2+} concentrations of 19.7 $\mu g\,m^{-3}$ (winter) and 12.9 $\mu g\,m^{-3}$ (spring). The Ca^{2+} levels during dust events were over double of seasonal average values for both PM$_{10}$ and PM$_{2.5}$ and this phenomenon was consistent with the report of previous literatures (*Wang et al., 2013*; *Shen et al., 2014*). Box plot variations of NO$_3^-$/SO$_4^{2-}$, Cl$^-$/K$^+$, OC/EC, and SO$_4^{2-}$/K$^+$ ratios have been also presented (Fig. 3) the average SO$_4^{2-}$/K$^+$ ratios were 19.8 for PM$_{10}$ and 18.0 for PM$_{2.5}$. High SO$_4^{2-}$/K$^+$ ratio indicated important coal combustion contribution to PM. In addition, Cl$^-$/K$^+$ ratios were 3.1.

The highest PM$_{2.5}$ OC/EC ratios was observed during summer (5.2), followed by spring (3.9), winter (3.7), and autumn (3.0), which was consistent with the value as *Cao et al. (2012a)* illustrated. The regressions between OC and EC in PM$_{10}$ and PM$_{2.5}$ were plotted as shown, respectively (Fig. S1). Most spots of the PM$_{10}$ and PM$_{2.5}$ OC/EC ratios are displayed under the coal combustion line, which indicated important contribution of coal combustion (*Cao et al., 2005*). Strong correlation coefficients (R) of 0.87 for PM$_{10}$ and 0.86 for PM$_{2.5}$ were found between OC and EC. High correlations (Fig. S2) showed cations and anions were the major ions extracted from the PM samples. The seasonal A/C ratios were 0.8, 0.8, 0.6, and 0.7. The major fraction of deficit anions in spring should be carbonate concentration (CO$_3^{2-}$) (*Shen et al., 2007*; *Shen et al., 2009*). Material balance (Fig. S3) in the following parts revealed that mineral dust was one of major components in aerosol
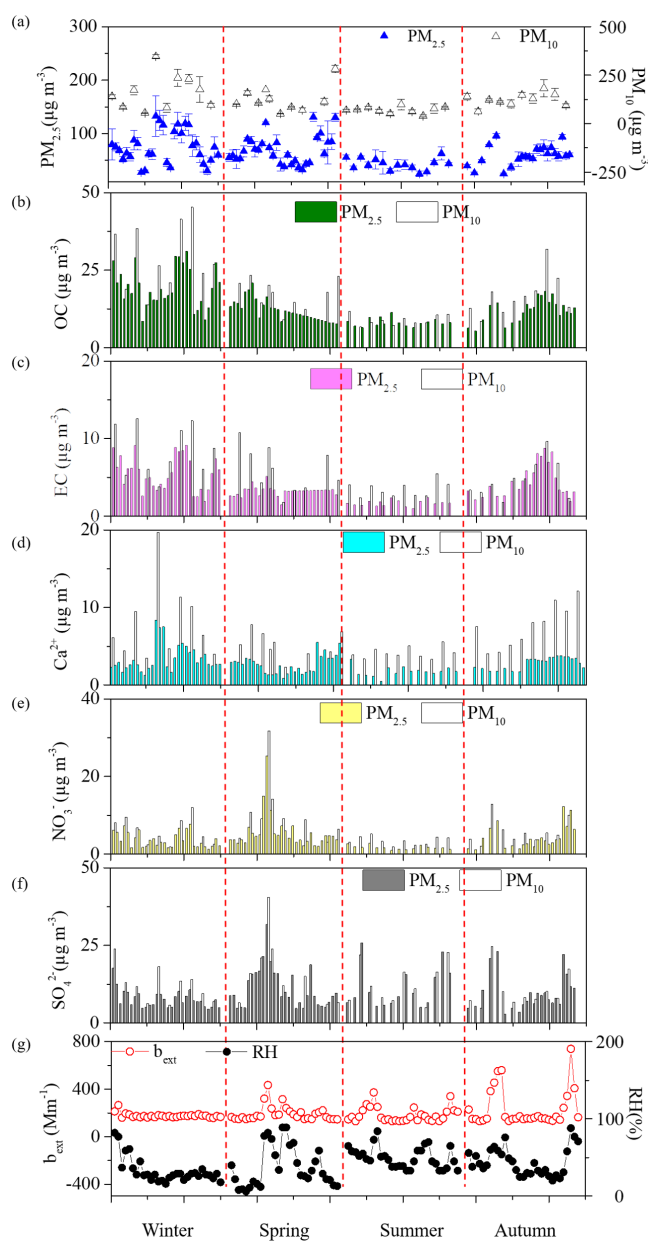
Figure 2 Temporal variations of (A) PM and their chemical components of (B) OC, (C) EC, (D) Ca^{2+}, (E) NO_3^-, (F) SO_4^{2-}, and (G) bext and RH at Yulin during four seasons.

particle mass, and strong PM alkaline should attribute to high dust loading. A triangular diagram was created to show clearly the neutralization contribution of these three cations (Fig. S4). The yearly mean NF values of Ca^{2+}, NH_4^+, and Mg^{2+} were 0.25, 0.17, and 0.02. It was clear that Ca^{2+} and NH_4^+ were the major neutralizers.
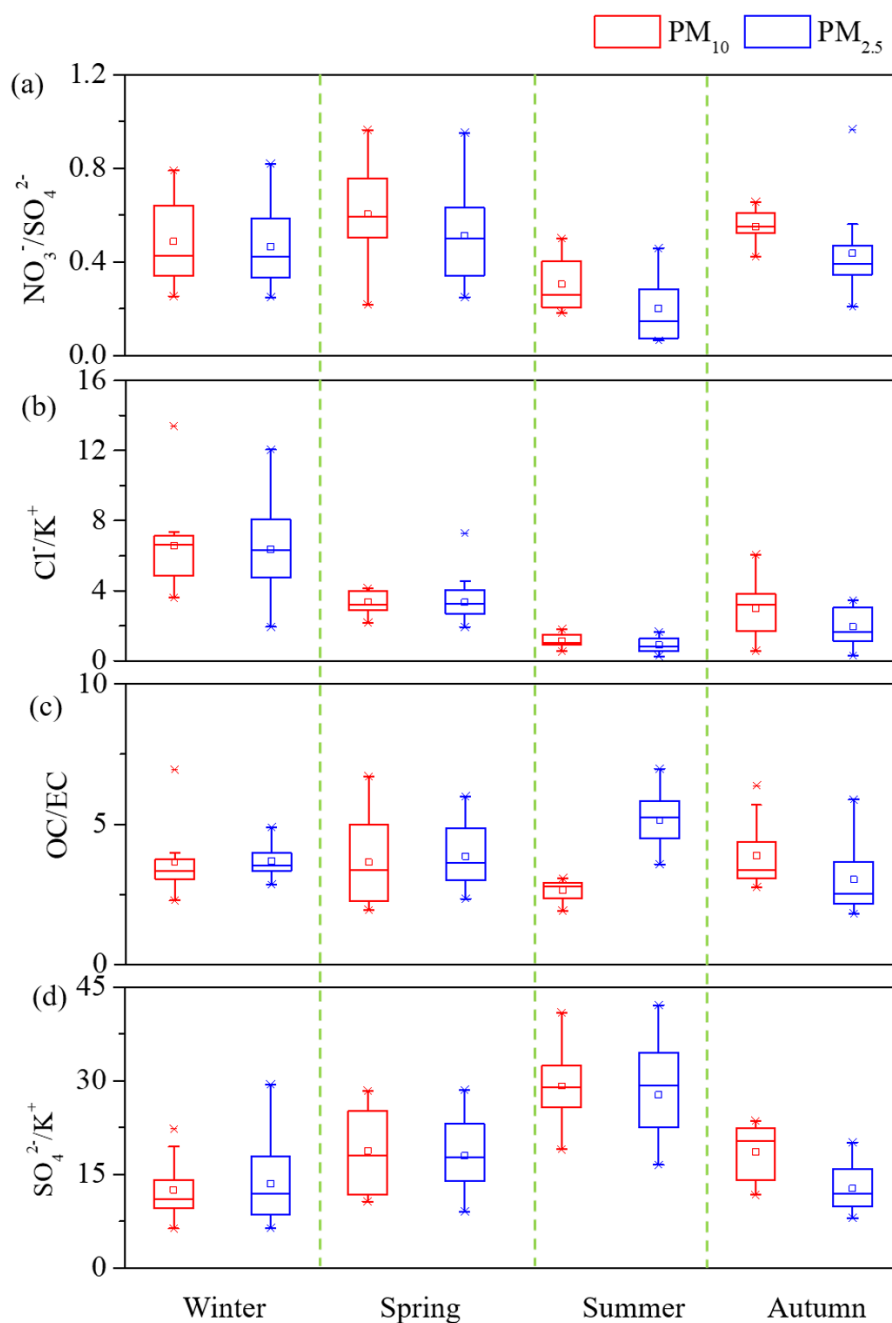
Figure 3 Box plot (10th, 25th, 50th, 75th, and 90th percentile; square pots: mean values) variations of (A) NO_3^-/SO_4^{2-}, (B) Cl^-/K^+, (C) OC/EC and (D) SO_4^{2-}/K^+ of PM.

Seasonal variations and source apportionment of light extinction

Daily averaged VR (Table S2) was 21.6 ± 7.3 km. Wind speeds (2.9 m s^{-1} for both spring and summer) and temperature (13 °C for spring and 23 °C for summer) inferred higher mixing and dispersion than those during winter. As shown in Table 2, winter b_{ext} (calculated from section 2.3) showed the highest with an average of 232.95 ± 154.88 Mm^{-1}, followed

Table 2 PCA performed on PM components, resulting in four independent factors.

Chemical species	PM$_{10}$				PM$_{2.5}$			
	Factor 1	Factor 2	Factor 3	Factor 4	Factor 1	Factor 2	Factor 3	Factor 4
Na$^+$	0.655	−0.048	0.617	−0.335	0.627	−0.224	0.443	−0.285
NH$_4^+$	0.287	0.893	−0.145	0.226	0.201	0.951	0.107	−0.035
K$^+$	0.69	0.386	0.318	−0.237	0.687	0.521	0.199	−0.185
Mg^{2+}	0.55	−0.313	0.589	0.226	0.337	−0.416	0.693	−0.265
Ca^{2+}	0.683	−0.37	0.414	0.186	0.408	−0.485	0.537	−0.221
F$^-$	0.752	−0.024	−0.115	−0.384	0.665	−0.35	−0.118	−0.169
Cl$^-$	0.813	0.008	0.262	−0.389	0.885	−0.117	−0.033	0.093
NO$_3^-$	0.374	0.776	0.209	0.174	0.343	0.735	0.372	−0.023
SO$_4^{2-}$	0.923	0.849	0.274	0.194	0.896	0.893	0.229	−0.096
OC1	0.773	0.07	−0.443	−0.238	0.898	−0.113	−0.196	−0.033
OC2	0.892	0.035	−0.33	0.058	0.908	0.091	−0.108	0.242
OC3	0.886	−0.123	−0.165	0.12	0.932	−0.058	−0.132	0.153
OC4	0.944	−0.221	−0.066	0.063	0.914	−0.097	−0.126	0.023
EC1	0.895	−0.014	−0.346	−0.024	0.912	0.057	−0.243	0.001
EC2	0.716	−0.114	−0.14	0.329	0.707	−0.212	0.081	0.366
EC3	0.531	−0.39	0.102	0.546	0.01	−0.017	0.653	0.712
OP	0.916	−0.003	−0.276	0.029	0.828	0.225	−0.314	−0.099
% Var	23.9	7.6	58.1	7.3	27.8	11.3	47.1	3.6

Notes.

% Var, percentage of the variance explained by each factor.

the decrease order of autumn >summer >spring, which were similar in Xi'an (*Cao et al., 2012b*).

According to section 3.1 and mass balance results (Fig.S2), (NH$_4$)$_2$SO$_4$, NH$_4$NO$_3$, OM, EC, the major contributors to PM. Moreover, coarse matter (CM) was important contributor to b_{ext} as a result of high PM$_{10}$ concentrations (*Cao et al., 2012a*). In this study, unidentified chemical species were summed up and revered as "Others" below. In general, the b_{ext} can be estimated statistically as follows:

$$b_{ext} = a_1[CM] + a_2[OM] + a_3[EC] + a_4 f_L(RH)[NH_4NO_3] + a_5 f_L(RH)[(NH_4)_2SO_4]$$
$$+ others \tag{14}$$

b_{ext} and chemical species mass concentrations are presented with the Mm^{-1} and µg m^{-3} unit, respectively. $f_L(RH)$ is the growth curves of sulfate and nitrate, which can be found in IMPROVE net results (*Pitchford et al., 2007*). $f_L(RH)$ was used in this study because sulfate and nitrate mass are distributed in droplet mode.

Potential sources and transport pathways of PM$_{2.5}$

In order to investigate the PM$_{2.5}$ potential advection, PSCF analysis was conducted in this study (*Petit et al., 2017*). Figure 4 shows the PCSF analysis results from December 2013 to October 2014, which suggested that local emissions, as well as certain regional transport from northwesterly and southerly areas, contributed to PM$_{2.5}$ loadings during the whole year. As average PM$_{2.5}$ values were lower than 75 µg m^{-3} in summer, some differences
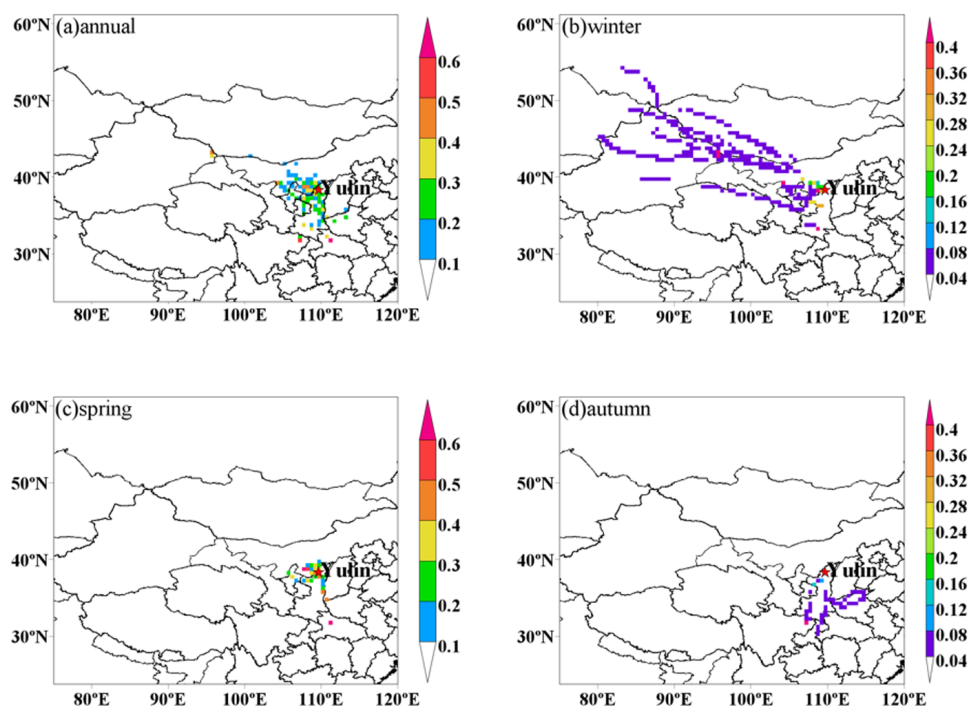
Figure 4 Potential source areas for PM$_{2.5}$ in Yulin during (A) annual, (B) winter, (C) spring, and (D) autumn. The color code denotes the PSCF probability. The measurement site is indicated with a red circle.

were found during the other three seasons. During winter, the potential source area has been recorded; it was mainly from local emissions. Besides, low potential source area was from the northwestern plain areas of Ningxia Hui Autonomous Region and Xinjiang Uyghur Autonomous Region. In contrast to winter, higher potential source regions for PM$_{2.5}$ during spring stretched to local emissions and the juncture of Guanzhong Plain, Henan province, Inner Mongolia and Ningxia Hui Autonomous Region.

Source apportionment of PM

In this study, PCA analyses have been conducted to apportion the PM sources. The fundamental principle of PCA is that a strong correlation may exist between components from the same source. It searches factors that play the leading roles by analysis of correlation and variance. Multivariate factor analysis was adopted to help identification of dominant source categories and the results obtained by varimax rotated factor analysis for both PM$_{10}$ and PM$_{2.5}$ are presented in Table 3.

The fugitive dust was the most major source of PM, followed by coal combustion & gasoline vehicle emissions, secondary inorganic aerosol, and diesel vehicle emissions for both PM$_{10}$ and PM$_{2.5}$ (Fig. 5). For PM$_{10}$, Factor 1 was responsible for 23.9% of the total variance and had highly positive contributions from SO$_4^{2-}$, Cl$^-$, OC four fractions, EC1, EC2, and OP, indicating its relation to coal combustion and gasoline vehicle emission (*Huang et al., 2013*). Factor 2 (7.6% of the total variance) had highly correlation with

Table 3 PCA with varimax rotation for PM components data.

Chemical species	PM$_{10}$					PM$_{2.5}$				
	Factor 1	Factor 2	Factor 3	Factor 4	Communality	Factor 1	Factor 2	Factor 3	Factor 4	Communality
Na$^+$	0.655	0.048	0.617	0.335	0.8234	0.627	0.224	0.443	0.285	0.8189
NH$_4^+$	0.287	**0.893**	0.145	0.226	0.8434	0.201	**0.951**	0.107	0.035	0.8674
K$^+$	0.69	0.386	0.318	0.237	0.9123	0.687	0.521	0.199	0.185	0.9312
Mg^{2+}	0.55	0.313	**0.589**	0.226	0.8822	0.337	0.416	**0.693**	0.265	0.8659
Ca^{2+}	0.683	−0.37	**0.414**	0.186	0.8956	0.408	0.485	**0.537**	0.221	0.9187
F$^-$	0.752	0.024	0.115	0.384	0.9231	0.665	−0.35	0.118	0.169	0.9052
Cl$^-$	**0.813**	0.008	0.262	0.389	0.9453	**0.885**	0.117	0.033	0.093	0.9312
NO$_3^-$	0.374	**0.776**	0.209	0.174	0.9204	0.343	**0.735**	0.372	0.023	0.9124
SO$_4^{2-}$	**0.923**	**0.849**	0.274	0.194	0.9663	**0.896**	**0.893**	0.229	0.096	0.9645
OC1	**0.773**	0.07	0.443	0.238	0.8154	**0.898**	0.113	0.196	0.033	0.8069
OC2	**0.892**	0.035	−0.33	0.058	0.8798	**0.908**	0.091	0.108	0.242	0.8123
OC3	**0.886**	0.123	0.165	0.12	0.8332	**0.932**	0.058	0.132	0.153	0.8397
OC4	**0.944**	0.221	0.066	0.063	0.8120	**0.914**	0.097	0.126	0.023	0.8189
EC1	**0.895**	0.014	0.346	0.024	0.8987	**0.912**	0.057	0.243	0.001	0.8759
EC2	**0.716**	0.114	−0.14	0.329	0.8824	**0.707**	0.212	0.081	0.366	0.9325
EC3	0.531	−0.39	0.102	**0.546**	0.7923	0.01	0.017	0.653	**0.712**	0.8261
OP	**0.916**	0.003	0.276	0.029	0.8090	**0.828**	0.225	0.314	0.099	0.8267
% Var	23.9	7.6	58.1	7.3	Total 96.9%	27.8	11.3	47.1	3.6	Total 89.8%
Eigen value	5.34	3.45	2.67	1.6		6.52	2.87	2.91	1.23	

Notes.

% Var, percentage of the variance explained by each factor.

NH$_4^+$, SO$_4^{2-}$, and NO$_3^-$, which represented the source of secondary inorganic aerosols (*Shen et al., 2011*). The fugitive dust was a main contributor to PM$_{10}$, with a contribution of 58.1% (*Zhang et al., 2014*). Factor 4 should be responsible for 7.3% of the total variance and had highly positive contributions from EC3, indicating its relation to diesel vehicle exhaust (*Shen et al., 2011*). However, PM$_{2.5}$ showed some differences. Factors 1, 2, 3, and 4 represented the source of, diesel exhaust, coal combustion& gasoline exhaust, secondary inorganic aerosols, fugitive dust and diesel vehicle exhaust, accounting for 27.8%, 11.3%, 47.1% and 3.6% of the total variance, respectively.

The source apportionments of PM were presented in Fig. 5. PM$_{10}$ showed a maximum contribution of 49.0% from fugitive dust. The coal combustion& gasoline vehicle emissions contributed 20.2%, while the contribution from secondary inorganic aerosols and diesel vehicle exhaust were found to be 6.7% and 8.6%, respectively. In the case of PM$_{2.5}$, 39.4% of the mass has been contributed by 39.4% and 22.3% from coal combustion& gasoline vehicle emissions. Secondary inorganic aerosol contributed to 9.1% and 11.8% for diesel vehicle exhaust.
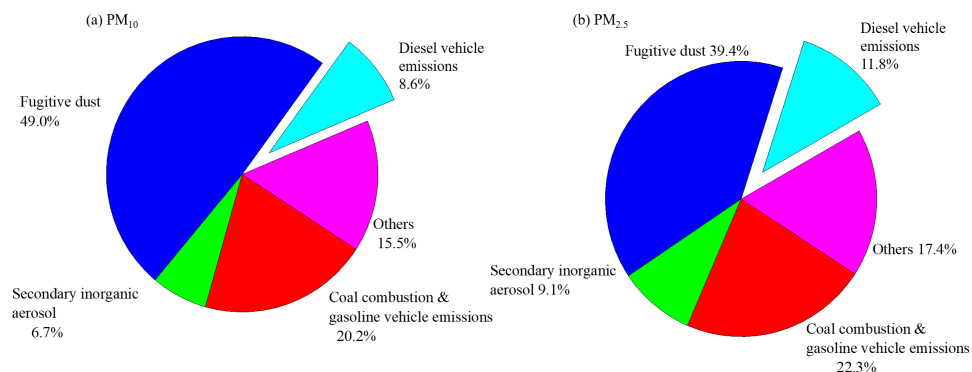
Figure 5 Source contribution analyses for (A) PM$_{10}$ and (B) PM$_{2.5}$ defined by PCA analyses.

DISCUSSION

On a basis of a record of data analysis, this study has demonstrated that fossil fuel especially coal consumption should lead to the high PM pollutions in Yulin. In fact, in our previous study, lower NO$_3^-$/SO$_4^{2-}$ ratio suggests that stationary emission of coal combustion was the dominant source of PM particle (*Lei et al., 2018*). Coal burning in power plant and resident heating should be the major source of high sulfate. In addition, Industry emissions such as coke production also contributed to high sulfate. Sulfate, the most abundance component, highlighted coal combustion contribution to PM.

As Yulin is located in the cross border between desert and the Chinese loess, high spring PM levels should attribute to increasing of eolian dust. Prior studies also reported that heavy dust storm events in Yulin led to high TSP levels in spring of 257 µg m^{-3} (*Zhang et al., 2003*). In contrast, cities far away from the desert showed a different seasonal pattern compared to Yulin. High Ca^{2+} levels in winter and autumn should attribute to urban fugitive dust emitted by high wind from road and construction sites. The domestic heating period in Yulin started from November 1 to April 30 the next year. One hand, high SO$_4^{2-}$ concentrations observed during spring was mainly due to the domestic heat. The average wind speed and RH were 2.86 m s^{-1} and 38%, which were a little higher than those during summer. However, the temperature during spring was 13 °C, which could enhance the strong gas-particle transfer conversions of SO$_2$ to SO$_4^{2-}$. In contrast, high summer sulfate should mainly due to high temperature enhancing the strong gas-particle transfer conversions of SO$_2$ to SO$_4^{2-}$, as suggested in some studies (*Wang et al., 2012*; *Shen et al., 2014*). Winter lower SO$_4^{2-}$ levels attribute to high wind speed (2.56 m s^{-1} in average) favorable to diffusion and low relative humidity (33% in average) unfavorable to sulfate formation. High winter and low spring sulfate were observed in Xi'an, which showed a difference seasonal pattern when compared to Yulin (*Shen et al., 2014*). High winter sulfate was due to coal combustion in heating season and unfavorable diffusion condition in Xi'an (low wind speed, averaged 1.45 m s^{-1}, and high RH, 55.9% in average). Lower NO$_3^-$/SO$_4^{2-}$ ratio suggests that stationary emissions are a dominant source of PM

particles which has also been reported in *Lei et al. (2018)*. Summer NO_3^-/SO_4^{2-} ratios were the lowest for both PM_{10} and $PM_{2.5}$, which because high temperature can favor SO_2 converted to SO_4^{2-}, while low RH was unfavorable the NO_3^- formation (*Shen et al., 2008*). High SO_4^{2-}/K^+ and Cl^-/K^+ ratios indicated important coal combustion contribution to PM (*Shen et al., 2009*).

High summer $PM_{2.5}$ OC/EC ratio inferred a dominant fraction of OC from gas-particle conversion. In fact, high temperature and atmospheric oxidation in summer favored the secondary organic carbon (SOC) formation (*Wang et al., 2012*). The regressions between OC and EC in PM_{10} and $PM_{2.5}$ were plotted as shown, respectively (Fig. S1). Most spots of the PM_{10} and $PM_{2.5}$ OC/EC ratios are displayed under the coal combustion line, which indicated important contribution of coal combustion (*Cao et al., 2005*). High sulfate and OC levels also supported our conclusion. The regression equation intercepts for $PM_{2.5}$ and PM_{10}, indicated that OC primary non-combustion emissions, such as regional background carbonaceous species, long range transport, and local biological detritus, influenced heavily on fine particles in comparison with coarse fraction (*Turpin & Huntzicker, 1995*). Seasonal A/C ratios variations showed that spring PM samples were more alkaline because of the high loadings of Ca^{2+} and Mg^{2+} (*Shen et al., 2014*). The neutralization contributions illustrated that low contribution of Mg^{2+} changed the PM from weakly acidic to weakly alkaline in many PM samples.

Good correlations in different seasons were found between the reconstructed b_{ext} and the b_{ext} estimated by visibility (Fig. S5). A summary of the light extinction source apportionment results were presented in Table 2. On average, CM, NH_4NO_3 and$(NH_4)_2SO_4$ were the most chemical species contributing to b_{ext}. $(NH_4)_2SO_4$ accounted highest in summer (34.39 ± 14.79%), while NH_4NO_3showed the large contribution in autumn. During winter, $(NH_4)_2SO_4$ also was the highest during winter followed by CM. These results indicated that the extinction effects from $(NH_4)_2SO_4$ and NH_4NO_3 significantly increased under high RH conditions during summer and winter.

PSCF results have shown that dust was the most abundant components during spring, which was due to the atmospheric dust transport. Unlike winter and spring, potential source area was mainly from local emissions and low potential source areas were from northerly areas like Guanzhong Plain. This is consistent with the dominant source from coal combustion related above (*Liu et al., 2015*). PCA results showed the fugitive dust and coal combustion dominated the PM loadings both in PM_{10} and $PM_{2.5}$ over Yulin. Moreover, local emissions and some certain regional transport were the main sources. Despite the dust transportation, the economic boom in Yulin gave rise to substantial air pollution. In order to improve the air quality, strict measurements should be launched in both local and regional areas.

CONCLUSIONS

The chemical species for PM were analyzed and their associated sources were identified in Yulin, China. PM levels, OC, EC were highest during winter and lowest during summer. High Ca^{2+} levels during winter and autumn should attribute to fugitive dust. High spring

and summer sulfate levels should be due to different sources. Ion balance illustrated that PM_{10} samples were more alkaline than $PM_{2.5}$. Winter b_{ext} showed the highest with an average of 232.95 ± 154.88 Mm^{-1}, followed by autumn, summer, and spring. The regression equation intercepts for different values in $PM_{2.5}$ and PM_{10} indicated that OC primary non-combustion emissions, such as regional background carbonaceous species, long range transport, and local biological detritus, influenced heavily on fine particles in comparison with coarse fraction. Light extinction source apportionment results inferred that the extinction effects from hygroscopic species, such as, $(NH_4)_2SO_4$, NH_4NO_3, increased significantly under high RH conditions during summer and winter. High SO_4^{2-}/K^+ and Cl^-/K^+ ratio indicated the important contribution of coal combustion. PCA analyses results showed that the fugitive dust was the most major source of PM, followed by coal combustion & gasoline vehicle emissions, secondary inorganic aerosol and diesel vehicle emissions. PSCF results suggested that $PM_{2.5}$ were mainly from both local emissions and regional transport from northwesterly and southerly areas during the whole year.

ACKNOWLEDGEMENTS

We are thankful for the permission and coordination of Yulin Environmental Monitoring Station.

Funding

This research was supported by the National Natural Science Foundation of China (41877383, 41573101) and State Key Laboratory of Loess and Quaternary Geology, Institute of Earth Environment, CAS (SKLLQG1616). The funders had no role in study design, data collection and analysis, decision to publish, or preparation of the manuscript.

Grant Disclosures

The following grant information was disclosed by the authors:
National Natural Science Foundation of China: 41877383, 41573101.
State Key Laboratory of Loess and Quaternary Geology, Institute of Earth Environment, CAS: SKLLQG1616.

Competing Interests

The authors declare there are no competing interests.

Author Contributions

- Yali Lei conceived and designed the experiments, performed the experiments, analyzed the data, prepared figures and/or tables, and approved the final draft.
- Zhenxing Shen conceived and designed the experiments, analyzed the data, authored or reviewed drafts of the paper, and approved the final draft.
- Zhuoyue Tang and Jian Sun performed the experiments, prepared figures and/or tables, and approved the final draft.

- Qian Zhang conceived and designed the experiments, performed the experiments, prepared figures and/or tables, and approved the final draft.
- Yongjing Ma and Xiaoyan Wu analyzed the data, prepared figures and/or tables, and approved the final draft.
- Yiming Qin analyzed the data, prepared figures and/or tables, authored or reviewed drafts of the paper, and approved the final draft.
- Hongmei Xu and Renjian Zhang conceived and designed the experiments, authored or reviewed drafts of the paper, and approved the final draft.

Field Study Permissions

The following information was supplied relating to field study approvals (i.e., approving body and any reference numbers): All the field work have been permitted by the Yulin Environmental Monitoring Station (20150915).

Data Availability

The following information was supplied regarding data availability: The raw measurements are available in the Supplemental Files.

Supplemental Information

Supplemental information for this article can be found online at http://dx.doi.org/10.7717/peerj.8447#supplemental-information.

REFERENCES

Cao J, Lee S, Ho K, Zhang X, Zou S, Fung K, Chow J, Watson J. 2003. Characteristics of carbonaceous aerosol in Pearl River Delta Region, China during 2001 winter period. *Atmospheric Environment* **37**:1451–1460 DOI 10.1016/S1352-2310(02)01002-6.

Cao J, Shen Z, Chow J, Qi G, Watson J. 2009. Seasonal variations and sources of mass and chemical composition for PM_{10} aerosol in Hangzhou, China. *Particuology* **7**:161–168 DOI 10.1016/j.partic.2009.01.009.

Cao J, Shen Z, Chow J, Watson J, Lee S, Tie X, Ho K, Wang G, Han Y. 2012a. Winter and summer $PM_{2.5}$ chemical compositions in fourteen Chinese cities. *Journal of the Air & Waste Management Association* **62**:1214–1226 DOI 10.1080/10962247.2012.701193.

Cao J, Wang Q, Chow J, Watson J, Tie X, Shen Z, Wang P, An Z. 2012b. Impact of aerosol compositions on visibility impairment in Xi'an, China. *Atmospheric Environment* **59**:559–566 DOI 10.1016/j.atmosenv.2012.05.036.

Cao J, Wu F, Chow J, Lee S, Li Y, Chen S, An Z, Fung K, Watson J, Zhu C, Liu S. 2005. Characterization and source apportionment of atmospheric organic and elemental carbon during fall and winter of 2003 in Xi'an, China. *Atmospheric Chemistry and Physics* **5**:3127–3137 DOI 10.5194/acp-5-3127-2005.

Charlson R, Schwartz S, Hales J, Cess R, Coakley J, Hansen J, Hofmann D. 1992. Climate forcing by anthropogenic aerosols. *Science* **255**:423–430 DOI 10.1126/science.255.5043.423.

Chow J, Bachmann J, Wierman S, Mathai C, Malm W, White W, Mueller P, Kumar N, Watson J. 2002. Critical review discussion-visibility: science and regulation. *Journal of the Air & Waste Management Association* **52**:973–999 DOI 10.1080/10473289.2002.10470844.

Chow J, Watson J. 1999. Ion chromatography in elemental analysis of airborne particles. *Elemental Analysis of Airborne Particles* **1**:97–137.

Chow J, Watson J, Chen L, Chang M, Robinson N, Trimble D, Kohl S. 2007. The IMPROVE-A temperature protocol for thermal/optical carbon analysis: maintaining consistency with a long-term database. *Journal of the Air & Waste Management Association* **57**:1014–1023 DOI 10.3155/1047-3289.57.9.1014.

Chow J, Watson J, Green M, Frank N. 2010. Filter light attenuation as a surrogate for elemental carbon. *Journal of the Air & Waste Management Association* **60**:1365–1375 DOI 10.3155/1047-3289.60.11.1365.

Hodkinson J. 1966. Calculations of colour and visibility in urban atmospheres polluted by gaseous NO2. *Air & Water Pollution* **10**:137–144.

Huang B, Liu M, Ren Z, Bi X, Zhang G, Sheng G, Fu J. 2013. Chemical composition, diurnal variation and sources of PM2.5, at two industrial sites of South China. *Atmospheric Pollution Research* **4**:298–305 DOI 10.5094/APR.2013.033.

Huang R, Zhang Y, Bozzetti C, Ho K, Cao J, Han Y, Daellenbach K, Slowik J, Platt S, Canonaco F, Zotter P, Wolf R, Pieber S, Bruns E, Crippa M, Ciarelli G, Piazzalunga A, Schwikowski M, Abbaszade G, Kreis J, Zimmermann R, An Z, Szidat S, Baltensperger U, Haddad I, Prevot A. 2014. High secondary aerosol contribution to particulate pollution during haze events in China. *Nature* **514**:218–222 DOI 10.1038/nature13774.

Ji D, Gao W, Maenhaut W, He J, Wang Z, Li J, Du W, Wang L, Sun Y, Xin J, Hu B. 2019. Impact of air pollution control measures and regional transport on carbonaceous aerosols in fine particulate matter in urban Beijing, China: insights gained from long-term measurement. *Atmospheric Chemistry and Physics* **19**:8569–8590 DOI 10.5194/acp-19-8569-2019.

John W, Wall S, Ondo J, Winklmayr W. 1990. Modes in the size distributions of atmospheric inorganic aerosol. *Atmospheric Environment* **24**:2349–2359 DOI 10.1016/0960-1686(90)90327-J.

Koschmieder H. 1924. Theorie der horizontalen sichtweite, Beitrage zur Physik der Freien Atmosphare. *Meteorologische Zeitschrift Z* **12**:3353.

Lee S, Ghim Y, Kim S, Yoon S. 2009. Seasonal characteristics of chemically apportioned aerosol optical properties at Seoul and Gosan, Korea. *Atmospheric Environment* **243**:1320–1328 DOI 10.1016/j.atmosenv.2008.11.044.

Lei Y, Shen Z, Wang Q, Zhang T, Cao J, Sun J, Zhang Q, Wang L, Xu H, Tian J, Wu J. 2018. Optical characteristics and source apportionment of brown carbon in winter $PM_{2.5}$ over Yulin in Northern China. *Atmospheric Research* **213**:27–33 DOI 10.1016/j.atmosres.2018.05.018.

Liu F, Zhang Q, Tong D, Zheng B, Li M, Huo H, He K. 2015. High-resolution inventory of technologies, activities, and emissions of coal-fired power plants

in China from 1990 to 2010. *Atmospheric Chemistry Physics* **15**:13299–13317
DOI 10.5194/acp-15-13299-2015.

Meng C, Wang L, Zhang F, Wei Z, Ma S, Ma X, Yang J. 2015. Characteristics of concentrations and water-soluble inorganic ions in $PM_{2.5}$ in Handan City, Hebei province, China. *Atmospheric Research* **171**:133–146
DOI 10.1016/j.atmosres.2015.12.013.

Petit J, Favez O, Albinet A, Canonaco F. 2017. A user-friendly tool for comprehensive evaluation of the geographical origins of atmospheric pollution: wind and trajectory analyses. *Environmental Modelling & Software* **88**:183–187
DOI 10.1016/j.envsoft.2016.11.022.

Pitchford M, Malm W, Schichtel B, Kumar N, Lowenthal D, Hand J. 2007. Revised algorithm for estimating light extinction from IMPROVE particle speciation data. *Journal of the Air & Waste Management Association* **57**:1326–1336
DOI 10.3155/1047-3289.57.11.1326.

Polissar A, Hopke P, Harris J. 2001. Source regions for atmospheric aerosol measured at Barrow, Alaska. *Environmental Science & Technology* **35**:4214–4226
DOI 10.1021/es0107529.

Shen Z, Arimoto R, Cao J, Zhang R, Li X, Du N, Okuda T, Nakao S, Tanaka S. 2008. Seasonal variations and evidence for the effectiveness of pollution controls on water-soluble inorganic species in total suspended particulates an fine particulate matter from Xi'an, China. *Journal of the Air & Waste Management Association* **58**:1560–1570 DOI 10.3155/1047-3289.58.12.1560.

Shen Z, Cao J, Arimoto R, Han Z, Zhang R, Han Y, Liu S, Okuda T, Nakao S, Tanaka S. 2009. Ionic composition of TSP and $PM_{2.5}$ during dust storms and air pollution. *Atmospheric Environment* **43**:2911–2918 DOI 10.1016/j.atmosenv.2009.03.005.

Shen Z, Cao J, Arimoto R, Zhang R, Jie D, Liu S, Zhu C. 2007. Chemical composition and source characterization of spring aerosol over Horqin sand land in northeastern China. *Journal of Geophysical Research: Atmosphere* **112(D14)**
DOI 10.1029/2006JD007991.

Shen Z, Cao J, Liu S, Zhu C, Wang X, Zhang T, Xu H, Hu T. 2011. Chemical composition of PM_{10} and $PM_{2.5}$ collected at ground level and 100 m during a strong winter time pollution episode in Xi'an, China. *Journal of the Air & Waste Management Association* **61**:1150–1159 DOI 10.1080/10473289.2011.608619.

Shen Z, Cao J, Zhang L, Liu L, Zhang Q, Li J, Han Y, Zhu C, Zhao Z, Liu S. 2014. Day-night differences and seasonal variations of chemical species in PM_{10} over Xi'an, northwest China. *Environmental Science & Pollution Research* **21**:3697–3705
DOI 10.1007/s11356-013-2352-z.

Shen Z, Zhang L, Cao J, Tian J, Liu L, Wang G, Zhao Z, Wang X, Zhang R, Liu S. 2012. Chemical composition, sources, and deposition fluxes of water-soluble inorganic ions obtained from precipitation chemistry measurements collected at an urban site in northwest China. *Journal of Environmental Monitoring* **14**:3000–3008
DOI 10.1039/c2em30457k.

Tao J, Zhang L, Gao J, Wang H, Chai F, Wang S. 2015. Aerosol chemical composition and light scattering during a winter season in Beijing. *Atmospheric Environment* **110**:36–44 DOI 10.1016/j.atmosenv.2015.03.037.

Taylor S, McLenna S. 1985. *The continental crust: its composition and evolution.* Oxford: Blackwell, 315.

Turpin B, Huntzicker J. 1995. Identification of secondary organic aerosol episodes and quantitation of primary and secondary organic aerosol concentrations during SCAQS. *Atmospheric Environment* **29**:3527–3544 DOI 10.1016/1352-2310(94)00276-Q.

Viana M, Querol X, Alastuey A, Gil J, Menende M. 2006. Identification of PM sources by principal component analysis (PCA) coupled with wind direction data. *Chemosphere* **65**:2411–2418 DOI 10.1016/j.chemosphere.2006.04.060.

Wang Q, Cao J, Shen Z, Tao J, Xiao S, Luo L, He Q, Tang X. 2013. Chemical composition of $PM_{2.5}$ during dust storms and air pollution events in Chengdu, China. *Particuology* **11**:70–77 DOI 10.1016/j.partic.2012.08.001.

Wang X, Shen Z, Cao J, Zhang L, Liu L, Li J, Liu S, Sun Y. 2012. Characteristics of surface ozone at an urban site over Xi'an in Northwest China. *Journal of Environmental Monitoring* **14**:116–126 DOI 10.1039/C1EM10541H.

Watson J. 2002. Visibility: science and regulation. *Journal of the Air & Waste Management Association* **52**:628–713 DOI 10.1080/10473289.2002.10470813.

Xu J, Bergin M, Greenwald R, Schauer J, Shafer M, Jaffrezo J, Aymoz G. 2004. Aerosol chemical, physical, and radiative characteristics near a desert source region of northwest China during ACE-Asia. *Journal of Geophysical Research* **109**:D19 DOI 10.1029/2003JD004239.

Yuan C, Lee C, Liu S, Chang J, Yuan C, Yang H. 2006. Correlation of atmospheric visibility with chemical composition Kaohsiung aerosols. *Atmospheric Research* **82**:663–679 DOI 10.1016/j.atmosres.2006.02.027.

Zhang Q, Shen Z, Cao J, Ho K, Zhang R, Bie Z, Chang H, Liu S. 2014. Chemical profiles of urban fugitive dust over Xi'an in the south margin of the Loess Plateau, China. *Atmospheric Pollution Research* **5**(**3**):421–430 DOI 10.5094/APR.2014.049.

Zhang X, Gong S, Shen Z, Mei F, Xi X, Liu L, Zhou Z, Wang D, Wang Y, Cheng Y. 2003. Characterization of soil dust aerosol in China and its transport and distribution during 2001 ACE-Asia: 1. Network observations. *Journal of Geophysical Research* **108**:D9 DOI 10.1029/2002JD002632.